Hindawi
Complexity
Volume 2019, Article ID 2319560, 10 pages
https://doi.org/10.1155/2019/2319560

Research Article

A Variable Structure Control Scheme Proposal for the Tokamak à Configuration Variable

Aitor Marco,[1] **Aitor J. Garrido**,[2] **Stefano Coda**,[3] **Izaskun Garrido**,[2] **and TCV Team**

[1]*Advanced Design & Analysis Department, IDOM, Bilbao, Spain*
[2]*Automatic Control Group, ACG, Institute of Research and Development of Processes, IIDP, Automatic Control and Systems Engineering Department, University of Basque Country (UPV/EHU) Bilbao, Spain*
[3]*Ecole Polytechnique Fédérale de Lausanne (EPFL), Swiss Plasma Center (SPC), CH-1015 Lausanne, Switzerland*

Correspondence should be addressed to Aitor Marco; aitor.marco@idom.com

Received 25 October 2018; Revised 7 January 2019; Accepted 10 February 2019; Published 14 April 2019

Academic Editor: Yan-Ling Wei

Fusion power is the most significant prospects in the long-term future of energy in the sense that it composes a potentially clean, cheap, and unlimited power source that would substitute the widespread traditional nonrenewable energies, reducing the geographical dependence on their sources as well as avoiding collateral environmental impacts. Although the nuclear fusion research started in the earlier part of 20th century and the fusion reactors have been developed since the 1950s, the fusion reaction processes achieved have not yet obtained net power, since the generated plasma requires more energy to achieve and remain in necessary particular pressure and temperature conditions than the produced profitable energy. For this purpose, the plasma has to be confined inside a vacuum vessel, as it is the case of the Tokamak reactor, which consists of a device that generates magnetic fields within a toroidal chamber, being one of the most promising solutions nowadays. However, the Tokamak reactors still have several issues such as the presence of plasma instabilities that provokes a decay of the fusion reaction and, consequently, a reduction in the pulse duration. In this sense, since long pulse reactions are the key to produce net power, the use of robust and fast controllers arises as a useful tool to deal with the unpredictability and the small time constant of the plasma behavior. In this context, this article focuses on the application of robust control laws to improve the controllability of the plasma current, a crucial parameter during the plasma heating and confinement processes. In particular, a variable structure control scheme based on sliding surfaces, namely, a sliding mode controller (SMC) is presented and applied to the plasma current control problem. In order to test the validity and goodness of the proposed controller, its behavior is compared to that of the traditional PID schemes applied in these systems, using the RZIp model for the Tokamak à Configuration Variable (TCV) reactor. The obtained results are very promising, leading to consider this controller as a strong candidate to enhance the performance of the PID-based controllers usually employed in this kind of systems.

1. Introduction

Traditional nonrenewable energy sources are called to play a minor role in the near future, due to the increasing demand for energy in the world and the limited resources present on the planet. Other factors that have also an impact on this kind of energies are the pollution provoked by the carbon-based fuels, such as petroleum or coal, as well as the nuclear waste and risks originated by the fission reactors. However, nowadays the nonrenewable energies still represent the 86% of the world total primary energy supply [1]. The renewable energies are being developed and improved for the purpose of increasing their efficiency and ensuring that all the energy needs are covered. The biomass, hydroelectric, solar, and the wind power are some of the most widely used renewable energies, but they suffer from several issues such as intermittency and dispersion, or pollution in the case of biomass. Besides, they usually require subsidies, large areas to be located, and sometimes rare-earth materials.

In this context, the most promising solution to meet the world energy needs is the fusion power, which presents many advantages compared to the fission power: the resources needed are virtually unlimited on Earth, the nuclear waste is limited—just short-live activated materials of the reactor are

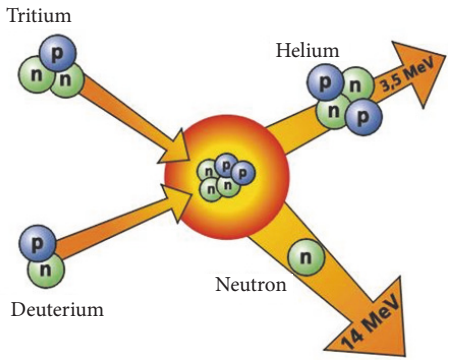

Figure 1: D-T fusion reaction.

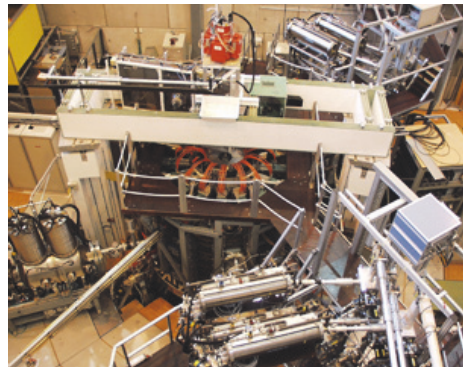

Figure 2: TCV reactor.

generated, some of which could be reused as fuel—there is no risk of nuclear explosion or disaster, and the fusion reaction provides the largest amount of energy per kilogram of fuel used. The nuclear fusion consists in artificially provoking the combination of light atom nuclei such as deuterium and tritium (Figure 1). This reaction releases a huge amount of energy, which can be used to heat water and drive a turbine and generate electricity.

The main disadvantages of the fusion power are the large quantity of energy needed to start and hold the reaction and the short duration of the plasma achieved until now. This article tackles this issue by developing advanced controls so as to increase the confinement time and energy availability.

In order to test the feasibility of the nuclear fusion as a power source, an experimental fusion reactor called ITER (International Thermonuclear Experimental Reactor) [2] has been promoted by an international consortium formed by the European Union, China, Japan, India, South Korea, Russia, and the United States. ITER considers a Tokamak fusion reactor that confines the hot plasma in a toroidal chamber using high magnetic fields. The ITER project will test all elements required for the construction of a functional fusion reactor such as the breeder blanket modules, which will provide the tritium obtained from lithium, needed for the D-T reaction. Once the new technologies have been tested, a new reactor, namely, DEMO [3], will be built to demonstrate that the production of energy is feasible.

ITER and DEMO are being planned, developed, and built, while several small Tokamaks serve as a test bench to research the fusion power [4], such as the Globus-M Spherical Tokamak [5] in Russia or the Joint European Torus (JET) [6] in Europe which is the world's largest Tokamak with 38 MW of heating power and 100 m^3 of plasma volume. Another interesting operational experimental fusion reactor is the Tokamak à Configuration Variable (TCV) [7], a control-oriented research fusion reactor of the Ecole Polytechnique Fédérale de Lausanne (EPFL), shown in Figure 2, whose main objective is the study of the plasma shape.

Nowadays, the current controller in the TCV and in most of the experimental Tokamaks is the traditional Proportional-Integral-Derivative controller (PID) which has proved to solve the main instabilities problems of the fusion reaction in the Tokamaks but not the major disruptions which are still an inherent issue of them [8–12]. In this context, this article seeks to maximize pulse length by making use of a new control scheme for the plasma current. The model for plasma current, position, and shape to be used is based on the RZIp and extracted from real experimental data of TCV.

Table 1: TCV coils.

Types	# Coils	Power Source
Toroidal Field Coils	16	1
OH Coils	7	2
Shaping Coils	16	16
In-vessel Vertical fb Coils	2	1

The TCV reactor, despite its small size of 1.54 m height by 0.56 width, is a very complex machine, fully loaded of sensors (the so-called diagnostics) and actuators, as it can be seen in Figure 3. Among the diagnostics, there are some for the measurement of the spatial profiles of the electron temperature and density, such as the Thomson Scattering Diagnostic [13], or for the measurement for the plasma currents, temperature, density, and potential, such as the Langmuir probes [14], whose locations are illustrated in Figure 4. The data obtained from some diagnostics (as well as many others related to the plasma physics) are processed and serve as input for the control system, which can actuate over different types of actuators, the Electron Cyclotron Resonance Heating and Current Drive System (ECRH-ECCD), the gas valves, and the coils. The coils are the main actuators for the plasma control, as gathered in Table 1, and there are 4 types with 41 total number of coils fed with 20 independent power sources. Currently, the control system of the TCV is fed with 128 input signals from the diagnostics, which are linearly transformed into 24 observers. This set of observers is composed of the plasma current I_p, the PF coil currents, the difference between the currents in the two Ohmic coil circuits, the vertical position estimator, the radial position estimator, an elongation estimator, and the line-integrated density. With these observables and the reference signals, 24 error signals are generated and serve as input to a PID controller whose outputs are the required voltages for the coils [8, 9]. The scope of this article is to enhance the current PID controller that acts in one of these observers, the plasma current, a relevant parameter to achieve and maintain the fusion reaction. It

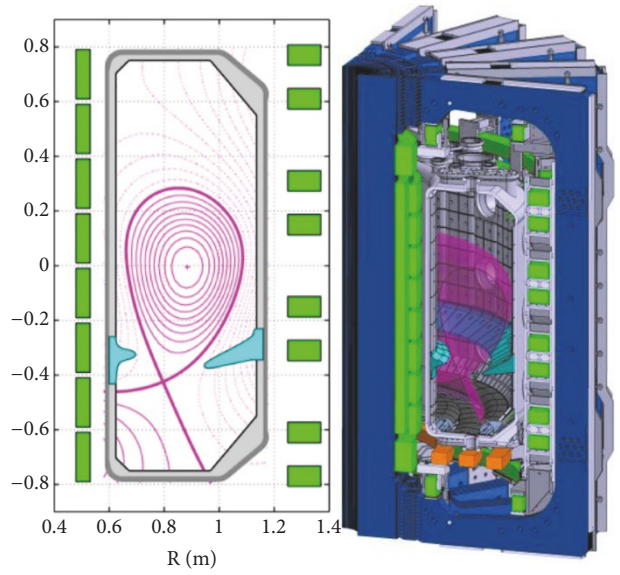

Figure 3: TCV reactor section.

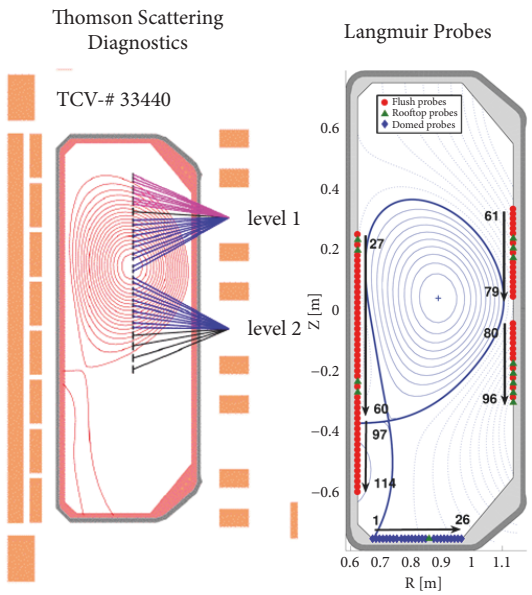

Figure 4: TCV diagnostics.

is obvious that better control implies a better response of the system and instability corrections, which may extend the duration of the pulses. The sliding mode control scheme has been studied in this article to enhance the actual control system, which is a variable structure control that presents a robust behavior against plant uncertainties and a finite-time convergence. To test the improvements of this new control scheme, a simulation based on real experimental data has been performed with Simulink.

The remainder of this article is organized as follows: Section 2 introduces the TCV system and explains the RZIp model. In Section 3, the simulation model is presented and the proposed sliding mode control scheme is explained in detail. The Lyapunov stability is studied for the sliding mode controller in Section 4. Results and comparisons are given in Section 5. Section 6 gathers the concluding remarks.

2. System Description

Tokamaks are devices where the plasma is confined in a toroidal chamber by magnetic fields. These magnetic fields are created by two groups of coils:

(i) Poloidal field coils: There are coils along the torus that create the poloidal magnetic field. They control the plasma current and stabilize the plasma. In particular, the main coils that act on the plasma current are the OH coils (serving as primary winding like a transformer), which are divided into two sets where the control signals concerning this article will be input.

(ii) Toroidal field coils: There are coils set in poloidal planes that create a toroidal magnetic field. They control the shape of the plasma.

One of the main issues to overcome in the path to commercialization is the instabilities [15–24]. These instabilities cause disruptions, limiting the maximal achievable time for plasma confinement and making indispensable an optimal control system.

In order to develop the control system, a plant model is required. The TCV is simulated by the RZIp model [15], which considers a rigid plasma radial and vertical displacement. The RZIp model is widely used for simulation purposes and design of real time controllers [19–24].

The state variables of the model are the plasma current, $\boldsymbol{I_e}$, the structure currents, $\boldsymbol{I_s}$, and the radial, $\boldsymbol{R}$, and vertical, $\boldsymbol{z}$, position of the plasma (1):

$$\dot{\boldsymbol{q}} = \begin{bmatrix} \boldsymbol{I_e} \\ \boldsymbol{I_s} \\ \dot{\boldsymbol{r}} \end{bmatrix}, \quad \text{where } \boldsymbol{r} = \begin{bmatrix} \boldsymbol{R} \\ \boldsymbol{z} \end{bmatrix} \tag{1}$$

The input variables are the effective voltages applied to each plasma element, $\boldsymbol{V_e}$, and the external poloidal field coil voltages, $\boldsymbol{V_s}$, (2):

$$\boldsymbol{U} = \begin{bmatrix} \boldsymbol{V_e} \\ \boldsymbol{V_s} \\ \boldsymbol{0} \end{bmatrix}. \tag{2}$$

The RZIp model takes into account four vector equations, Kirchoff's voltage law for the plasma elements (3), Kirchoff's voltage law for the structural and poloidal circuits (4), and the force balance for the radial (5) and vertical (6) directions:

$$\frac{d\left(\boldsymbol{L_e I_e} + \boldsymbol{M_{es} I_s} + \boldsymbol{R E I_e}\right)}{dt} + \boldsymbol{\Omega_e I_e} = \boldsymbol{V_e}, \tag{3}$$

$$\frac{d\left(\boldsymbol{L_s I_s} + \boldsymbol{M_{se} I_e}\right)}{dt} + \boldsymbol{\Omega_s I_s} = \boldsymbol{V_s}, \tag{4}$$

$$\frac{d\left(\boldsymbol{m_e}\dot{\boldsymbol{R}}\right)}{dt} = \frac{1}{2}\boldsymbol{I_e'}\frac{\partial \boldsymbol{L_e}}{\partial \boldsymbol{R}}\boldsymbol{I_e} + \boldsymbol{I_s'}\frac{\partial \boldsymbol{M_{se}}}{\partial \boldsymbol{R}}\boldsymbol{I_e} + \frac{\boldsymbol{EI_e^2}}{2}, \tag{5}$$

$$\frac{d\left(\boldsymbol{m_e}\dot{\boldsymbol{z}}\right)}{dt} = \frac{1}{2}\boldsymbol{I_e'}\frac{\partial \boldsymbol{L_e}}{\partial \boldsymbol{z}}\boldsymbol{I_e} + \boldsymbol{I_s'}\frac{\partial \boldsymbol{M_{se}}}{\partial \boldsymbol{z}}\boldsymbol{I_e}. \tag{6}$$

where subindex e denotes the plasma elements, subindex s denotes the structural elements, $\boldsymbol{L}$ and $\boldsymbol{M}$ are the self and mutual inductance matrices, $\boldsymbol{\Omega}$ is the resistance matrix, $\boldsymbol{E}$ is a constant matrix, and the mass matrix $\boldsymbol{m_e}$ contains the mass of each plasma current elements. Due to the complexity and nonlinearity of the equations that describe the behavior of the system, it will be linearized and simplified around an operation point using real data from the experiments. In this article, the data used for the model and simulation have been obtained from the shot numbers #49626 and #57587 of the TCV and can be represented by the following state-space system:

$$\begin{aligned} \dot{\boldsymbol{x}}_{\boldsymbol{RZIp}} &= A\boldsymbol{x}_{\boldsymbol{RZIp}} + B\boldsymbol{u}_{\boldsymbol{RZIp}} \\ \boldsymbol{y}_{\boldsymbol{RZIp}} &= C\boldsymbol{x}_{\boldsymbol{RZIp}}. \end{aligned} \tag{7}$$

where $\boldsymbol{x}_{\boldsymbol{RZIp}}$ are the state vector, $\boldsymbol{u}_{\boldsymbol{RZIp}}$ are the input vector, which are the supplied voltages for the coils, $\boldsymbol{y}_{\boldsymbol{RZIp}}$ is the output vector that comprises the observers of the system including the plasma current, A is the state matrix, B is the input matrix, and C is the output matrix. As in $\boldsymbol{y}_{\boldsymbol{RZIp}}$ there are other variables that are out of the scope of this article and are not going to be controlled using the SMC algorithm, and the plasma current output may be obtained from $\boldsymbol{u}_{\boldsymbol{RZIp}}$ and expressed as $y_{Ip} = C_{Ip}\boldsymbol{y}_{\boldsymbol{RZIp}}$, where C_{Ip} selects the desired output, so that the state variables can be rewritten as

$$\boldsymbol{x}_{\boldsymbol{RZIp}} = \left(C_{Ip}C\right)^{-1} y_{Ip}. \tag{8}$$

Introducing (8) in (7), the state-space system can be reformulated as

$$\dot{y}_{Ip} = \left(C_{Ip}C\right) A \left(C_{Ip}C\right)^{-1} y_{Ip} + \left(C_{Ip}C\right) B\boldsymbol{u}_{\boldsymbol{RZIp}}. \tag{9}$$

The dynamic equation of the plasma current model may be written in a simplified way as

$$\dot{y}_{Ip} = ay_{Ip} + bu_{OH} - d \tag{10}$$

where u_{OH} is the input that controls the plasma current, d is the term that gathers all the uncertainties and noncontrollable inputs, and the state matrix can be reduced to a single scalar as follows:

$$a = \left(C_{Ip}C\right) A \left(C_{Ip}C\right)^{-1}. \tag{11}$$

The tracking error of the plasma current, e_{Ip}, is defined as the difference of plasma current reference, r_{Ip}, and its actual value:

$$e_{Ip} = r_{Ip} - y_{Ip}. \tag{12}$$

Deriving the tracking error and substituting the plasma current model described in (10), the following expression is obtained:

$$\dot{e}_{Ip} = \dot{r}_{Ip} - \dot{y}_{Ip} = ae_{Ip} + u + \delta \tag{13}$$

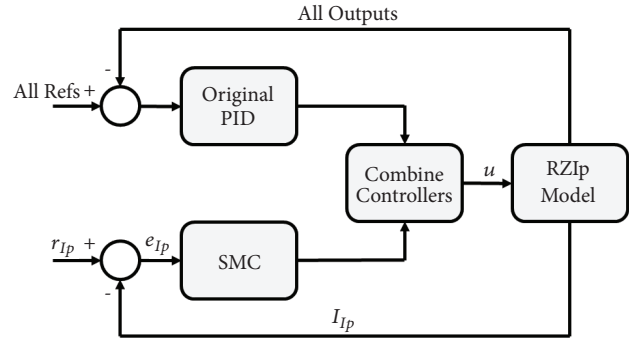

Figure 5: General overview of the model.

where the control signal, u, collects the following term:

$$u = -bu_{OH} \tag{14}$$

and the disturbances, uncertainties, and commands are gathered in δ:

$$\delta = d + \dot{r}_{Ip} - ar_{Ip}. \tag{15}$$

3. Sliding Mode Control Scheme

In order to improve the robustness of the TCV control system, the original PID has been enhanced with a sliding mode control for the plasma current, I_p. A schematic view of the general model may be observed in Figure 5, where in the box "SMC" the proposed sliding mode controller will be implemented and the resulting control signals will be combined in the box "Combine Controllers" [19, 24].

The sliding mode controller [25–27] uses a discontinuous control law to lead the system state to a specified sliding surface, σ, and to remain in it. This control law has two main advantages: the first is that the system behaves like a system of reduced order and the second is that the disturbances and uncertainties do not affect the movement on the sliding surface of the system. The development of the sliding control law is divided into two phases.

The first phase is to construct a sliding surface to confine the system dynamics to a sliding manifold with the desired behavior. Let us consider the ideal disturbance-free tracking error expression (13) and suppose that the trajectory of the state has intercepted the sliding surface σ at t_0, and exists a sliding mode at $t \geq t_0$ implying that $\sigma = 0$ and $\dot{\sigma} = 0$. Deriving σ with respect to time along the trajectory is defined by (13):

$$\dot{\sigma} = \left(\frac{\partial \sigma}{\partial e_{Ip}}\right)\dot{e}_{Ip} = \left(\frac{\partial \sigma}{\partial e_{Ip}}\right)\left(ae_{Ip} + u_{eq}\right) = 0 \tag{16}$$

where u_{eq} is the equivalent control, whose action entails that any trajectory starting at $\sigma = 0$ remains on it since $\dot{\sigma} = 0$. This equivalent control can be extracted from (16):

$$u_{eq} = -\left(\frac{\partial \sigma}{\partial e_{Ip}}\right)^{-1}\left(\frac{\partial \sigma}{\partial e_{Ip}}\right)ae_{Ip} = -ae_{Ip}. \tag{17}$$

Therefore, combining (13) and (17), given $\sigma(t_0) = 0$, the dynamics of the system on the sliding surface for $t \geq t_0$ are

$$\dot{e}_{Ip} = ae_{Ip} - ae_{Ip} = 0. \tag{18}$$

In this case, the sliding surface is computed with the error of the plasma current and its integral, taking the form of

$$\sigma = e_{Ip} + B \int e_{Ip} dt \tag{19}$$

where B is the relative weight between the integral of the error and the error of the plasma current.

The second phase is to design a discontinuous control law which is responsible for forcing the system to reach the sliding surface and maintains it there. For this reason, the control signal u is divided into two terms:

$$u = u_{eq} + u_N \tag{20}$$

where the continuous term u_{eq} is the equivalent control defined in (17) and u_N is the discontinuous term. In this particular case, the discontinuous term has been selected as a relay with state dependent gain, presenting the following expression:

$$u_N = -\beta \left(e_{Ip}\right) \text{sign}\left(\sigma\right) \tag{21}$$

where $\beta(e_{Ip}) > 0$ for all e_{Ip}. The term $\beta(e_{Ip})$ has been defined as

$$u_N = -\left(k_1 \left|e_{Ip}\right| + k_2 \left|\int e_{Ip} dt\right|\right) \text{sign}\left(\sigma\right). \tag{22}$$

Consequently, the control signal depends on the error of the plasma current and on the absolute value of the error and the integral of the error of the plasma current, and its sign is obtained from the sliding surface. This control signal is given by the following combining (17) and (22):

$$u = -k_c e_{Ip} - \left(k_1 \left|e_{Ip}\right| + k_2 \left|\int e_{Ip} dt\right|\right) \text{sign}\left(\sigma\right) \tag{23}$$

where k_c, k_1, and k_2 are tunable parameters.

The discontinuity of the sign function in $\sigma = 0$ leads to an undesirable chattering effect; thus the discontinuous transition is subject to smoothing. In order to obtain this smooth transition, the hyperbolic tangent of the sliding surface has been considered. So, the equation may be rewritten as follows:

$$u = -k_c e_{Ip} - \left(k_1 \left|e_{Ip}\right| + k_2 \left|\int e_{Ip} dt\right|\right) \tanh\left(\frac{\sigma}{k_t}\right) \tag{24}$$

where k_t is determined by the order of magnitude of the sliding surface.

Gathering (19) and (24), the sliding mode controller scheme is represented in Figure 6.

4. Lyapunov Stability

Rewrite the expression of the sliding surface σ, defined in (19), as

$$\sigma\left(t\right) = e_{Ip}\left(t\right) + \int_0^t \left(k - a\right) e_{Ip}\left(\tau\right) d\tau. \tag{25}$$

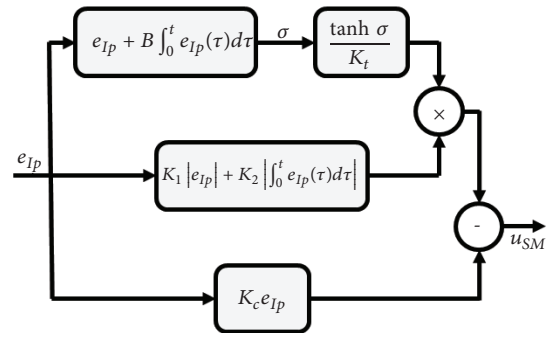

Figure 6: Sliding mode scheme.

So its derivative is

$$\dot{\sigma}\left(t\right) = \dot{e}_{Ip}\left(t\right) + \left(k - a\right) e_{Ip}\left(t\right). \tag{26}$$

Let us also recall the sliding mode controller law given in (23):

$$u\left(t\right) = -ke_{Ip}\left(t\right) - \beta \,\text{sign}\left(\sigma\left(t\right)\right). \tag{27}$$

In order to ensure the tracking capability, some assumptions shall be established:

(i) k shall be chosen so that the term $(k - \alpha)$ is strictly positive. Hence $k > \alpha$.

(ii) β shall be chosen so that $\beta \geq |\delta| \ \forall t$. To guarantee the robustness of the control action, a switching action is added with a size bigger than the perturbance. This condition implies that the uncertainties of the system are bounded magnitudes.

If the previous assumptions are verified and, using the Lyapunov stability theory, it is possible to demonstrate that the error of the plasma current defined in (12) tends to zero as time tends to infinity.

The Lyapunov function is defined by means of the following expression:

$$V = \frac{1}{2}\sigma\sigma \tag{28}$$

and its time derivative is

$$\begin{aligned} \dot{V} &= \sigma\dot{\sigma} = \sigma\left(\dot{e}_{Ip} + \left(k - a\right) e_{Ip}\right) = \sigma\left(ke_{Ip} + \delta + u\right) \\ &= \sigma\left(\delta - \beta \,\text{sign}\left(\sigma\right)\right) \leq -\left|\sigma\right|\left(\beta - \left|\delta\right|\right) \leq 0. \end{aligned} \tag{29}$$

As V is clearly positive definite, $\dot{V}$ is negative definite and when σ tends to infinity, V tends to infinity; then the equilibrium at the origin $\sigma = 0$ is globally asymptotically stable. This is to say, σ tends to zero as time tends to infinity, and all trajectories starting off $\sigma = 0$ must reach it in finite time and then remain on it, being in the so-called sliding mode.

5. Results

In order to validate the control scheme, the sliding mode controller has been simulated with a linearized RZIp model

Table 2: Simulated shots.

	#49626	#57587
Starting Time (s)	0.8	1
Duration (s)	0.5	0.5
Starting Ip (A)	-2.4E5	-2.8E5
Starting Radial Pos. (m)	0.872	0.879
Starting Vertical Pos. (m)	0.398	0.262

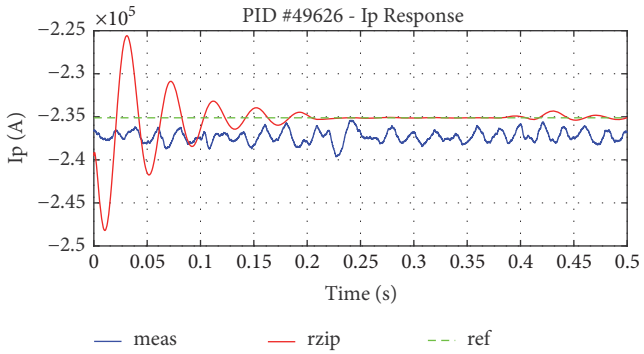

Figure 7: PID Response (Shot #49626).

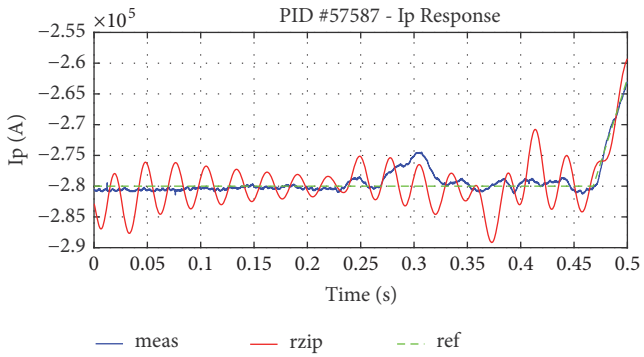

Figure 8: PID response (Shot #57587).

of the TCV and two distinct shots, #49626 and #57587, as shown in Table 2. The initial conditions of the system and the reference that the controller has to follow have also been obtained from the experimental data. In addition, to show the improvement of the new control scheme, the original PID controller has been implemented. The plasma current controller acts on the OH coils, which have a physical limit of ±1400 V, so the output has been saturated in case of overflow.

For a better comparison, the results have been divided into five groups: (A) system response, (B) RMS error, (C) integral error, and (D) control signals.

5.1. System Response. In Figures 7–10, the blue line represents the real measurement of the plasma current, the green dashed line is the reference commanded, and the red line is the response of the simulated system.

It can be clearly seen in Figures 7 and 8 that the original PID produces an underdamped response, which takes a long

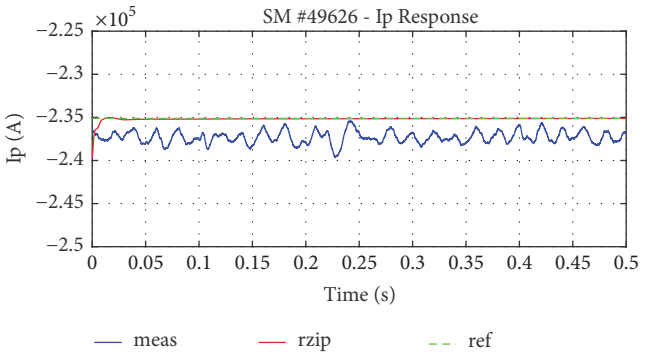

Figure 9: Sliding mode response (Shot #49626).

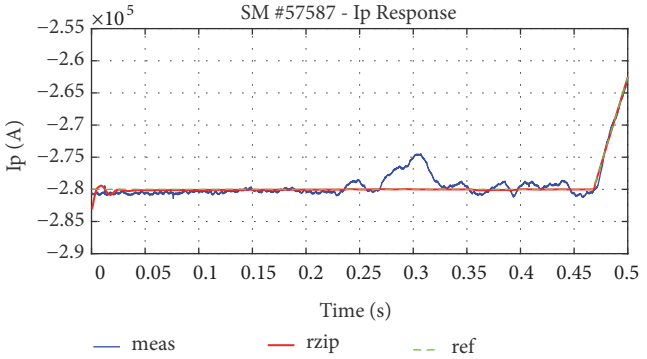

Figure 10: Sliding mode response (Shot #57587).

Table 3: RMS error.

Shot #	RMS PID	RMS Sliding Mode
49626	2.69E3	2.42E2
57587	3.12E3	2.18E2

time to reach the specified reference. This indicates that the response of the system may be subject to improvement.

The response of the sliding mode controller, shown in Figures 9 and 10, is better than that of the original PID controller because it reaches faster the reference with smaller oscillations. Even more, it may be seen that the response takes about the same time (10 ms) to start correcting the error and has an overshoot much smaller than using the PID.

5.2. RMS Error. One significant quantitative estimator is the Root Mean Square (RMS), which is a measure of the goodness of the controllers. The RMS for a discrete time series of the plasma current error with a fixed-time step can be computed with the following expression:

$$RMS_{e_{Ip}} = \sqrt{\frac{1}{N}\sum_{i=1}^{N} e_{Ip,i}^2}. \tag{30}$$

In Table 3, the RMS errors of the PID and the Sliding Mode controlled are depicted. The sliding mode controller reduces the RMS error by one order of magnitude.

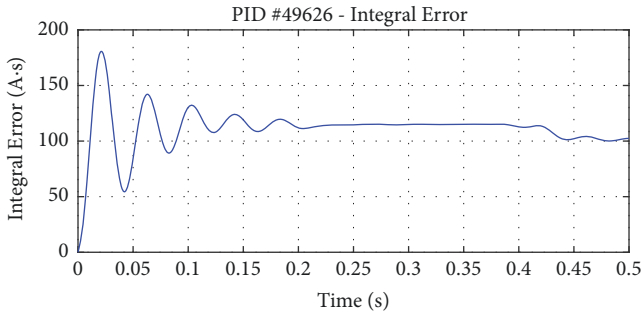

Figure 11: PID integral error (Shot #49626).

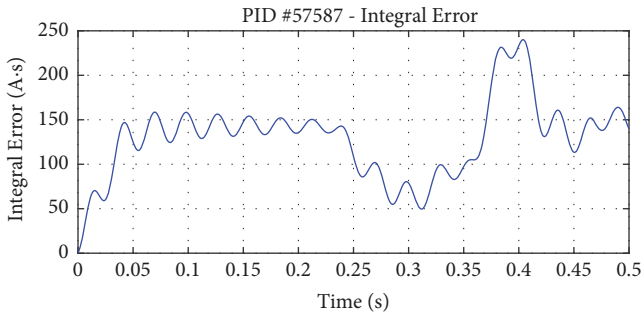

Figure 12: PID integral error (Shot #57587).

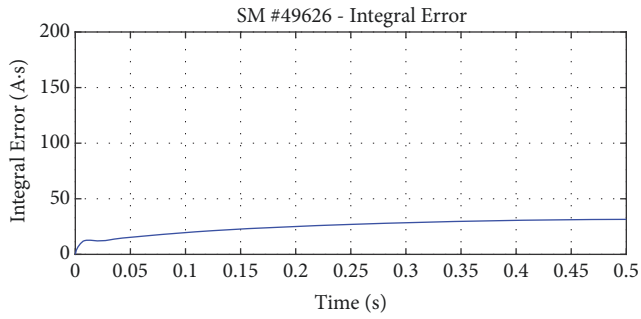

Figure 13: Sliding mode integral error (Shot #49626).

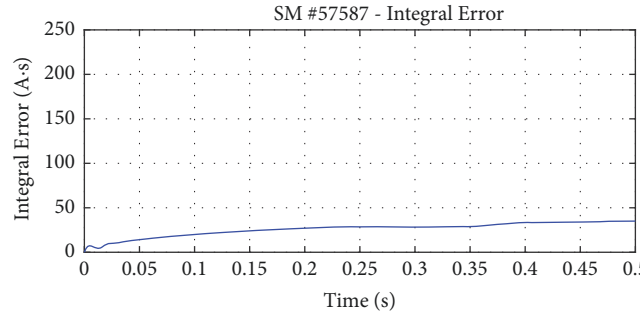

Figure 14: Sliding mode integral error (Shot #57587).

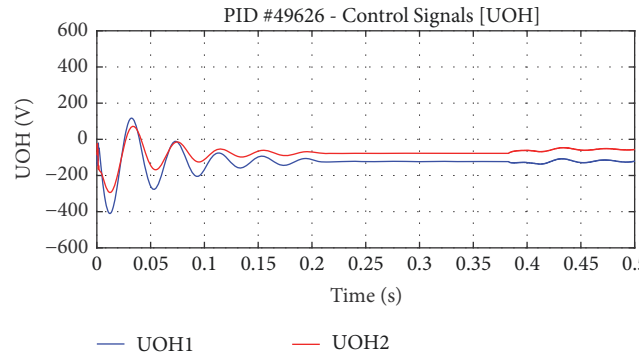

Figure 15: PID control signal (Shot #49626).

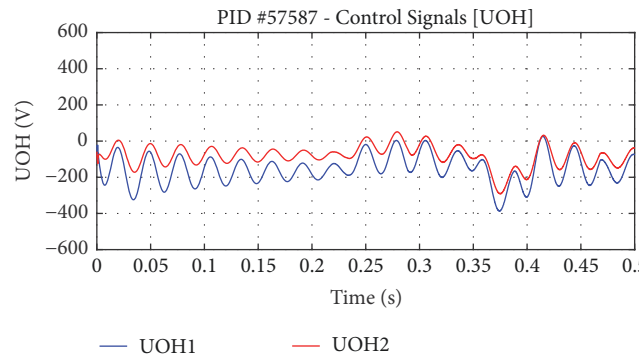

Figure 16: PID control signal (Shot #57587).

5.3. Integral Error. The integral error measures how the error accumulates along the time. It is clearly seen from Figures 11 and 12 that with the PID there are oscillations in the integral error.

However, in the integral error in the case of the sliding mode controller, as seen in Figures 13 and 14, there are no oscillations and the values are less than half of the PID's values.

5.4. Control Signals. It is important to keep in mind the feasibility of these controllers. The plasma current is controlled by two sets of OH coils, with a limit of ±1400 V for both. The difference between the control signals of the two sets is due to the controller of another plasma variable that is acting on them, which does not affect the performance of the plasma current response.

Figures 15 and 16 show the PID control signals, which have many oscillations until they reach the stationary state.

The sliding mode control signals are shown in Figures 17 and 18 where it can be seen that the oscillations are strongly reduced with a control effort smaller than that of the PID controller.

6. Conclusions

The use of optimal and robust control schemes seems to be one of the best ways to ensure an adequate control of the stability of the plasma, so as to extend the duration of the pulses. The traditional PID controllers now implemented within the Tokamak's control system do not allow achieving long enough duration pulses to enable energy production. In

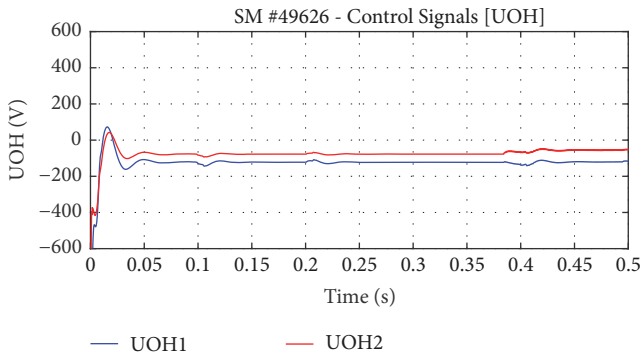

Figure 17: Sliding mode control signal (Shot #49626).

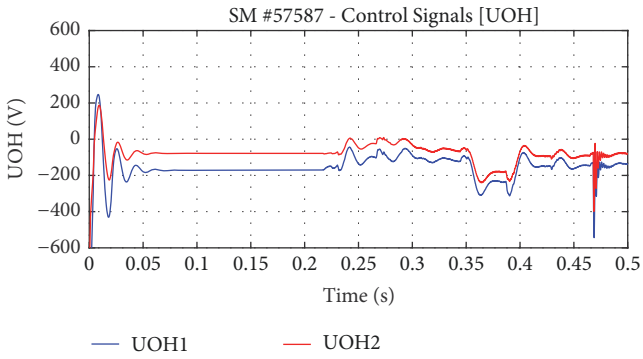

Figure 18: Sliding mode control signal (Shot #57587).

this context, new control laws have been developed and tested in order to obtain better results extending the pulse duration and making possible the production of fusion energy. The candidate proposed in this article to enhance the baseline PID-based scheme has been the sliding mode controller, which consists of a variable structure control law with low sensitivity to uncertainties.

As is shown from the results, the plasma current of the systems controlled by the original PID-based controller presents slow and underdamped oscillating responses. In contrast, the proposed sliding mode controller affords excellent results, with an improved fast system response and reduced oscillations of the plasma current, coupled with a more uniform control signal. Furthermore, the RMS errors of the sliding mode controller response show an order of magnitude improvement with respect to the PID ones.

Therefore, in view of the promising results gathered in this article, the next steps are to test them in different TCV scenarios to assure a good response of the controller in several situations and considering other external disturbances in the model that could be studied. In addition, parameter tuning algorithms, such as the Particle Swarm Optimization or the Water Cycle Algorithm, can be proposed.

Finally, the controllers should be tested in a real situation, implementing them at the 2019 experimental campaign of the TCV.

Appendix

The TCV Team is formed by:

S. Coda[1], J. Ahn[2], R. Albanese[3], S. Alberti[1], E. Alessi[4], S. Allan[5], H. Anand[1], G. Anastassiou[6], Y. Andrèbe[1], C. Angioni[7], M. Ariola[8], M. Bernert[7], M. Beurskens[9], W. Bin[4], P. Blanchard[1], T.C. Blanken[10], J.A. Boedo[11], T. Bolzonella[12], F. Bouquey[2], F.H. Braunmüller[1], H. Bufferand[2], P. Buratti[13], G. Calabró[13], Y. Camenen[14], D. Carnevale[15], F. Carpanese[1], F. Causa[13], R. Cesario[13], I.T. Chapman[5], O. Chellai[1], D. Choi[1], C. Cianfarani[13], G. Ciraolo[2], J. Citrin[16], S. Costea[17], F. Crisanti[13], N. Cruz[18], A. Czarnecka[19], J. Decker[1], G. De Masi[12], G. De Tommasi[3], D. Douai[2], M. Dunne[7], B.P. Duval[1], T. Eich[7], S. Elmore[5], B. Esposito[13], M. Faitsch[7], A. Fasoli[1], N. Fedorczak[2], F. Felici[10], O. Février[2], O. Ficker[20], S. Fietz[7], M. Fontana[1], L. Frassinetti[21], I. Furno[1], S. Galeani[15], A. Gallo[2], C. Galperti[1], S. Garavaglia[4], I. Garrido[22], B. Geiger[7,9], E. Giovannozzi[13], M. Gobbin[12], T.P. Goodman[1], G. Gorini[23], M. Gospodarczyk[15], G. Granucci[4], J.P. Graves[1], R. Guirlet[2], A. Hakola[24], C. Ham[5], J. Harrison[5], J. Hawke[1], P. Hennequin[25], B. Hnat[26,42], D. Hogeweij[16], J.-Ph. Hogge[1], C. Honoré[25], C. Hopf[7], J. Horáček[20], Z. Huang[1], V. Igochine[7], P. Innocente[12], C. Ionita Schrittwieser[17], H. Isliker[27], R. Jacquier[1], A. Jardin[2], J. Kamleitner[1], A. Karpushov[1], D.L. Keeling[5], N. Kirneva[28,29], M. Kong[1], M. Koubiti[14], J. Kovacic[30], A. Krämer-Flecken[31], N. Krawczyk[19], O. Kudlacek[7,12], B. Labit[1], E. Lazzaro[4], H.B. Le[1], B. Lipschultz[32], X. Llobet[1], B. Lomanowski[33], V.P. Loschiavo[3], T. Lunt[7], P. Maget[2], E. Maljaars[10], A. Malygin[1], M. Maraschek[7], C. Marini[1], P. Martin[12], Y. Martin[1], S. Mastrostefano[8], R. Maurizio[1], M. Mavridis[27], D. Mazon[2], R. McAdams[5], R. McDermott[7], A. Merle[1], H. Meyer[5], F. Militello[5], I.G. Miron[34], P.A. Molina Cabrera[1], J.-M. Moret[1], A. Moro[4], D. Moulton[5], V. Naulin[35], F. Nespoli[1], A.H. Nielsen[35], M. Nocente[23], R. Nouailletas[2], S. Nowak[4], T. Odstrčil[7], G. Papp[7], R. Papřok[20], A. Pau[36], G. Pautasso[7], V. Pericoli Ridolfini[8], P. Piovesan[12], C. Piron[12], T. Pisokas[27], L. Porte[1], M. Preynas[1], G. Ramogida[13], C. Rapson[7], J. Juul Rasmussen[35], M. Reich[7], H. Reimerdes[1], C. Reux[2], P. Ricci[1], D. Rittich[7], F. Riva[1], T. Robinson[5], S. Saarelma[5], F. Saint-Laurent[2], O. Sauter[1], R. Scannell[5], Ch. Schlatter[1], B. Schneider[17], P. Schneider[7], R. Schrittwieser[17], F. Sciortino[37], M. Sertoli[7], U. Sheikh[1], B. Sieglin[7], M. Silva[1], J. Sinha[1], C. Sozzi[4], M. Spolaore[12], T. Stange[9], T. Stoltzfus-Dueck[38], P. Tamain[2], A. Teplukhina[1], D. Testa[1], C. Theiler[1], A. Thornton[5], L. Tophøj[35], M.Q. Tran[1], C. Tsironis[6], C. Tsui[1,11], A. Uccello[4], S. Vartanian[2], G. Verdoolaege[39], K. Verhaegh[32], L. Vermare[25], N. Vianello[1,12], W.A.J. Vijvers[16], L. Vlahos[27], N.M.T. Vu[40], N. Walkden[5], T. Wauters[41], H. Weisen[1], M. Wischmeier[7], P. Zestanakis[6] and M. Zuin[12].

[1]Ecole Polytechnique Fédérale de Lausanne (EPFL), Swiss Plasma Center (SPC), CH-1015 Lausanne, Switzerland

[2]CEA, IRFM, F-13108 Saint Paul Lez Durance, France

[3]University of Napoli 'Federico II', Consorzio CREATE, Via Claudio 21, 80125 Napoli, Italy

[4]IFP-CNR, via R. Cozzi 53, 20125 Milano, Italy

[5]CCFE, Culham Science Centre, Abingdon, Oxon OX14 3DB, UK

[6]National Technical University of Athens, Athens, Greece
[7]Max-Planck-Institut für Plasmaphysik, D-85748 Garching, Germany
[8]University of Napoli Parthenope, Consorzio CREATE, Via Claudio 21, 80125 Napoli, Italy
[9]Max-Planck-Institut für Plasmaphysik, Teilinstitut Greifswald, D-17491 Greifswald, Germany
[10]Eindhoven University of Technology, P.O. Box 513, NL-5600 MB Eindhoven, Netherlands
[11]University of California, San Diego, Energy Research Center, La Jolla, CA 92093, USA
[12]Consorzio RFX, Corso Stati Uniti 4, 35127 Padova, Italy
[13]Unità Tecnica Fusione, ENEA C. R. Frascati, via E. Fermi 45, 00044 Frascati (Roma), Italy
[14]Aix-Marseille Université, CNRS, PIIM, F13013 Marseille, France
[15]University of Rome Tor Vergata, via del Politecnico 1, 00133 Rome, Italy
[16]FOM Institute DIFFER 'Dutch Institute for Fundamental Energy Research' Eindhoven, Netherlands
[17]Institut für Ionen- und Angewandte Physik, Universität Innsbruck, Technikerstraße 25, 6020 Innsbruck, Austria
[18]Instituto de Plasmas e Fusão Nuclear, Instituto Superior Técnico, Universidade de Lisboa, Lisbon, Portugal
[19]Institute of Plasma Physics and Laser Microfusion, Hery 23, 01-497 Warsaw, Poland
[20]Institute of Plasma Physics AS CR, Za Slovankou 1782/3, 182 00 Praha 8, Czechia
[21]Fusion Plasma Physics, EES, KTH, SE-10044 Stockholm, Sweden
[22]Faculty of Engineering, University of the Basque Country (UPV/EHU), Paseo Rafael Moreno 3, Bilbao 48013, Spain
[23]Department of Physics 'G. Occhialini', University of Milano-Bicocca, Piazza della Scienza 3, 20126 Milano, Italy
[24]VTT Technical Research Centre of Finland Ltd, P.O. Box 1000, FI-02044 VTT, Finland
[25]Laboratoire de Physique des Plasmas, CNRS UMR7648, Ecole Polytechnique, 91128 Palaiseau, France
[26]Rudolf Peierls Centre for Theoretical Physics, University of Oxford, Oxford, UK
[27]Aristotle University of Thessaloniki, Thessaloniki, Greece
[28]Institute of Physics of Tokamaks, National Research Center 'Kurchatov Institute', 123182 Kurchatov Sq., 1, Moscow, Russia
[29]National Research Nuclear University MEPhI (Moscow Engineering Physics Institute), 115409, Kashirskoe Sh., 31, Moscow, Russia
[30]Jožef Stefan Institute, Jamova 39, SI-1000 Ljubljana, Slovenia
[31]Forschungszentrum Jülich GmbH, Institut für Energie- und Klimaforschung, Plasmaphysik, 52425 Jülich, Germany
[32]Department of Physics, York Plasma Institute, University of York, Heslington, York YO10 5DD, UK
[33]Department of Physics, Durham University, Durham DH1 3LE, UK
[34]National Institute for Laser, Plasma and Radiation Physics, P.O. Box MG-36, Bucharest, Romania
[35]Department of Physics, Technical University of Denmark, Bldg 309, DK-2800 Kgs Lyngby, Denmark
[36]Department of Electrical and Electronic Engineering, University of Cagliari, Piazza d'Armi, 09123 Cagliari, Italy
[37]Plasma Science and Fusion Center, Massachusetts Institute of Technology, Cambridge, MA 02139, USA
[38]Princeton University, Princeton, NJ 08544, USA
[39]Department of Applied Physics, UG (Ghent University), St-Pietersnieuwstraat 41 B-9000 Ghent, Belgium
[40]Laboratoire de Conception et d'Intégration des Systèmes, Institut Polytechnique de Grenoble, BP54 26902 Valence Cedex 09, France
[41]Laboratory for Plasma Physics, Koninklijke Militaire School-Ecole Royale Militaire, Renaissancelaan 30 Avenue de la Renaissance, B-1000 Brussels, Belgium
[42]Culham Centre for Fusion Energy, Abingdon, UK.

Data Availability

The data used to support the findings of this study are available from the corresponding author upon request.

Conflicts of Interest

The authors declare that there are no conflicts of interest.

Acknowledgments

This work was supported by the MINECO through the Research Project DPI2015-70075-R (MINECO/FEDER, EU). The authors would like to thank the collaboration of the Spanish National Fusion Laboratory (EURATOM-CIEMAT) through Agreement UPV/EHUCIEMAT08/190 and EUSKAMPUS—Campus of International Excellence.

References

[1] Key World Energy Statistics, 2017, https://www.iea.org/publications/freepublications/publication/KeyWorld2017.pdf.
[2] N. Holtkamp, "An overview of the ITER project," *Fusion Engineering and Design*, vol. 82, no. 5–14, pp. 427–434, 2007.
[3] S. Ciattaglia et al., "The European DEMO fusion reactor: Design status and challenges from balance of plant point of view," in *Proceedings of the 2017 IEEE International Conference on Environment and Electrical Engineering and 2017 IEEE Industrial and Commercial Power Systems Europe (EEEIC / I&CPS Europe)*, pp. 1–6, Milan, Italy, June 2017.
[4] Y. Mitrishkin, P. Korenev, A. Prokhorov, N. Kartsev, and M. Patrov, "Plasma control in tokamaks. Part 1. controlled thermonuclear fusion problem. Tokamaks. Components of control systems," *Advances in Systems Science and Applications*, vol. 18, no. 2, pp. 26–52, 2018.
[5] V. K. Gusev et al., "Review of Globus-M spherical tokamak results," *Nuclear Fusion*, vol. 55, no. 10, Article ID 104016, 2015.
[6] X. Litaudon et al., "Overview of the JET results in support to ITER," *Nuclear Fusion*, vol. 57, no. 10, Article ID 102001, 2017.

[7] S. Coda et al., "Overview of the TCV tokamak program: scientific progress and facility upgrades," *Nuclear Fusion*, vol. 57, Article ID 102011, 2017.

[8] B. Duval, J. Moret, A. Rodrigues, L. Pereira, and C. Varandas, "Digital Control System for the TCV Tokamak," *IEEE Transactions on Nuclear Science*, vol. 53, no. 4, pp. 2179–2186, 2006.

[9] H. Le, F. Felici, J. Paley et al., "Distributed digital real-time control system for TCV tokamak," *Fusion Engineering and Design*, vol. 89, no. 3, pp. 155–164, 2014.

[10] M. Ariola and A. Pironti, *Magnetic Control of Tokamak Plasmas*, Springer, 2nd edition, 2016.

[11] Y. Mitrishkin, A. Prokhorov, P. Korenev, and M. Patrov, "Hierarchical robust switching control method with the Improved Moving Filaments equilibrium reconstruction code in the feedback for tokamak plasma shape," *Fusion Engineering and Design*, vol. 138, pp. 138–150, 2019.

[12] Y. V. Mitrishkin, N. M. Kartsev, E. A. Pavlova, A. A. Prokhorov, P. S. Korenev, and M. I. Patrov, "Plasma control in tokamaks. Part 2. Magnetic Plasma control systems," *Advances in Systems Science and Applications*, vol. 18, no. 3, pp. 39–78, 2018.

[13] G. Farias, S. Dormido-Canto, J. Vega et al., "Iterative noise removal from temperature and density profiles in the TJ-II Thomson scattering," *Fusion Engineering and Design*, vol. 89, no. 5, pp. 761–765, 2014.

[14] O. Février, C. Theiler, H. De Oliveira, B. Labit, N. Fedorczak, and A. Baillod, "Analysis of wall-embedded Langmuir probe signals in different conditions on the Tokamak à Configuration Variable," *Review of Scientific Instruments*, vol. 89, no. 5, p. 053502, 2018.

[15] A. S. Sharma, *Tokamak modeling and control [Doctoral Thesis]*, January 2002.

[16] I. Garrido, J. A. Romero, A. J. Garrido, D. Lucchin, E. Carrascal, and G. Sevillano-Berasategui, "Internal inductance predictive control for Tokamaks," in *Proceedings of the World Automation Congress (WAC '14)*, pp. 628–633, August 2014.

[17] M. G. Sevillano, I. Garrido, A. J. Garrido et al., "Observer-based real-time control for the poloidal beta of the plasma using diamagnetic measurements in tokamak fusion reactors," in *Proceedings of the IEEE Conference on Decision and Control*, pp. 7536–7542, December 2011.

[18] I. Garrido, A. J. Garrido, J. Romero, E. Carrascal, M. G. Sevillano, and O. Barambones, "Low effort Li nuclear fusion plasma control using model predictive control laws," *Mathematical Problems in Engineering*, vol. 2015, Article ID 527420, 8 pages, 2015.

[19] I. Garrido, A. Garrido, S. Coda, H. Le, and J. Moret, "Real time hybrid model predictive control for the current profile of the tokamak à configuration variable (TCV)," *Energies*, vol. 9, no. 8, p. 609, 2016.

[20] A. S. Sharma, D. J. N. Limebeer, I. M. Jaimoukha, and J. B. Lister, "Modeling and control of TCV," *IEEE Transactions on Control Systems Technology*, vol. 13, no. 3, Article ID 841647, pp. 356–369, 2005.

[21] I. Garrido, A. J. Garrido, O. Barambones, P. Alkorta, and F. J. Maseda, "Tokamak state-space control modeling," in *Proceedings of the 2008 Canadian Conference on Electrical and Computer Engineering - CCECE*, pp. 001437–001442, Niagara Falls, ON, Canada, May 2008.

[22] M. G. Sevillano-Berasategui, I. Garrido, A. J. Garrido, and O. Barambones, "Review of tokamak codes," in *Proceedings of the 5th International Conference on Electrical Engineering, Computing Science and Automatic Control (CCE)*, pp. 45–50, Mexico City, Mexico, November 2008.

[23] I. Garrido, A. Garrido, G. Sevillano, M. Alberdi, M. Amundarain, and O. Barambones, "Space-state modeling and control of tokamak reactors," *IFAC Proceedings Volumes*, vol. 42, no. 13, Part 1, pp. 431–436, 2009.

[24] I. Garrido, S. Coda, H. Le et al., "Hierarchical model predictive control in fusion reactors," in *Proceedings of the 2016 World Automation Congress (WAC)*, pp. 1–6, Rio Grande, PR, USA, July 2016.

[25] C. Vecchio, *Sliding mode control: theoretical developments and applications to uncertain mechanical systems [Doctoral Thesis]*, 2008.

[26] A. Levant, "Sliding order and sliding accuracy in sliding mode control," *International Journal of Control*, vol. 58, no. 6, pp. 1247–1263, 1993.

[27] A. Levant, "Higher-order sliding modes, differentiation and output-feedback control," *International Journal of Control*, vol. 76, no. 9-10, pp. 924–941, 2003.